

Thickness-dependent enhancement of damping in $\text{Co}_2\text{FeAl}/\beta\text{-Ta}$ thin films

Serkan Akansel,¹ Ankit Kumar,^{1,*} Nilamani Behera,¹ Sajid Husain,² Rimantas Brucas,¹ Sujeet Chaudhary,² and Peter Svedlindh¹

¹*Department of Engineering Sciences, Uppsala University, Box 534, SE-751 21 Uppsala, Sweden*

²*Thin Film Laboratory, Department of Physics, Indian Institute of Technology Delhi, New Delhi 110016, India*



(Received 5 March 2018; revised manuscript received 6 April 2018; published 23 April 2018)

In the present work Co_2FeAl (CFA) thin films were deposited by ion beam sputtering on Si (100) substrates at the optimized deposition temperature of 300 °C. A series of CFA films with different thicknesses (t_{CFA}), 8, 10, 12, 14, 16, 18, and 20 nm, were prepared and all samples were capped with a 5-nm-thick $\beta\text{-Ta}$ layer. The thickness-dependent static and dynamic properties of the films were studied by SQUID magnetometry, in-plane as well as out-of-plane broadband vector network analyzer–ferromagnetic resonance (FMR) measurements, and angle-dependent cavity FMR measurements. The saturation magnetization and the coercive field were found to be weakly thickness dependent and lie in the range 900–950 kA/m and 0.53–0.87 kA/m, respectively. The effective damping parameter (α_{eff}) extracted from in-plane and out-of-plane FMR results reveals a $\frac{1}{t_{\text{CFA}}}$ dependence, the values for the in-plane α_{eff} being larger due to two-magnon scattering (TMS). The origin of the α_{eff} thickness dependence is spin pumping into the nonmagnetic $\beta\text{-Ta}$ layer and in the case of the in-plane α_{eff} , also a thickness-dependent TMS contribution. From the out-of-plane FMR results, it was possible to disentangle the different contributions to α_{eff} and to extract values for the intrinsic Gilbert damping (α_G) and the effective spin-mixing conductance ($g_{\text{eff}}^{\uparrow\downarrow}$) of the CFA/ $\beta\text{-Ta}$ interface, yielding $\alpha_G = (1.1 \pm 0.2) \times 10^{-3}$ and $g_{\text{eff}}^{\uparrow\downarrow} = (2.90 \pm 0.10) \times 10^{19} \text{ m}^{-2}$.

DOI: [10.1103/PhysRevB.97.134421](https://doi.org/10.1103/PhysRevB.97.134421)

I. INTRODUCTION

Half-metallic ferromagnetic materials having a small Gilbert damping parameter (α), which describes the relaxation of the magnetization, are of immense interest for spin transfer torque devices since a low α value results in a low value for the critical current density required to switch the magnetization [1,2]. Co-based Heusler alloys, e.g., Co_2FeAl (CFA), have unique properties such as half-metallicity [3–5], large magnetization, and high Curie temperature ($T_C = 1000$ K) [5]. Their use as electrode material in magnetic tunnel junctions, due to giant tunneling magnetoresistance (360%) at room temperature, has been reported [6,7].

Full Heusler alloys, X_2YZ , can exhibit three different crystallographic phases—the fully ordered $L2_1$ phase, the partially ordered $B2$ phase, and the fully disordered $A2$ phase. In the $L2_1$ phase, the different types of atoms occupy their assigned sites, while in the partially ordered phase the Y and Z atoms randomly share sites. For the $A2$ phase, all available sites are occupied at random [8]. Unfortunately, crystallographic disorder reduces half-metallicity and increases the value of the Gilbert damping parameter. There exist a number of studies where postannealing has been utilized in order to obtain lower damping parameters. Damping parameters in the range from 0.001 to 0.004 have been obtained by postannealing of CFA films deposited on MgO substrates [8–14].

In the case of CFA films deposited on Si substrates [8,15,16] comparably few studies have been reported and the $B2$ phase is rarely achieved [15]. However, using ion beam sputtering and

optimizing the growth temperature, it has recently been shown that the $B2$ phase can be obtained without any postannealing process [17]. Besides obtaining the $B2$ phase, a record low value for the damping parameter for CFA films deposited on Si was reported.

The objective of this work is to investigate the thickness dependence of the magnetic relaxation for $B2$ phase Si/CFA/Ta thin films. Spin transfer torque devices typically require ultrathin magnetic electrode layers. One problem for devices is that decreasing the thickness of the magnetic layer often results in a concomitant increase of the magnetic damping parameter due to effects such as surface anisotropy [18]. The explanation for the increase of damping can be linked to the excitation of both uniform and nonuniform precession modes of the magnetization and, if a nonmagnetic layer with large spin-orbit coupling is used together with the magnetic layer, spin pumping into the nonmagnetic layer also contributes [19,20]. Uniform modes give rise to intrinsic or Gilbert type of relaxation, while nonuniform modes are known as extrinsic modes which can be caused by magnetic inhomogeneity or surface anisotropy fields. The nonuniform precession of the magnetic moments results in two-magnon scattering (TMS), where magnons are created. The TMS increases the linewidth of the ferromagnetic resonance (FMR) absorption as well as the effective damping parameter of the material [21,22]. The influence of surface/interface anisotropy is expected to increase by decreasing film thickness [23]. However, in out-of-plane FMR measurements, TMS is avoided and hence the effective damping parameter has a contribution from the intrinsic relaxation and can in addition exhibit a thickness-dependent spin-pumping contribution. The latter enhancement of the damping parameter has from theory been shown to

*ankit.kumar@angstrom.uu.se

be large for a ferromagnetic layer in direct contact with a nonmagnetic metal layer with large spin-orbit coupling (large spin-flip probability) [19,20]. Enhancement is thus expected for heavier elements with p and d electrons in the conduction band, while the enhancement will be absent for lighter elements as well as for heavier elements with only s electrons in the conduction band.

In this study CFA thin films capped with a high spin-orbit coupling $4d$ β -Ta layer have been investigated in terms of dynamic magnetization properties using both in-plane and out-of-plane FMR techniques to be able to distinguish between intrinsic and extrinsic contributions to the magnetic relaxation. Besides broadband FMR studies, angle-resolved cavity FMR measurements have also been utilized. The intrinsic damping parameter and the enhancement of damping due to TMS and spin pumping can be disentangled by angle-resolved and broadband FMR measurements, which is quite enlightening in terms of understanding the fundamental dynamical properties of these promising materials for future spintronic applications.

II. SAMPLES AND METHODS

CFA thin films were deposited on Si(100)/SiO₂ substrates by utilizing an ion beam sputtering deposition system (Nordiko-3450). Prior to deposition substrates were heat treated *in situ* at 620 °C for 2 h to remove surface contaminations. A base pressure of about 7×10^{-7} Torr was achieved by using cryo and turbo pumps. The Ar gas pressure was maintained at 2.4×10^{-4} Torr and the rf ion source was operated at 75 W during deposition. The film deposition technique is explained in detail in our previous work [17]. Films were grown at 300 °C. A series of films was prepared with the stacking Si/CFA(t_{CFA})/Ta(5 nm). Nominal t_{CFA} values were 8, 10, 12, 14, 16, 18, and 20 nm. All films were covered with a 5-nm-thick capping layer of β -Ta. The β -Ta layers were grown at room temperature and their quality was ascertained by x-ray diffraction and resistivity measurements [23].

Film thickness and surface/interface roughness were obtained by x-ray reflectivity (XRR) measurements. The scans covered the 2θ range 0° – 4° , and the XRR results were analyzed using the PANALYTICAL X'PERT REFLECTIVITY software package (ver. 1.2 with segmented fit). Layer thicknesses, densities, and surface/interface roughness were obtained from this analysis.

Magnetic hysteresis loop measurements were performed using a Magnetic Property Measurement System (MPMS, Quantum Design).

Dynamic magnetic properties were investigated both by fixed frequency cavity and broadband ferromagnetic resonance measurements. In the X-band cavity FMR measurements the frequency was kept constant at 9.8 GHz and an in-plane magnetic field was scanned during the measurement. The setup was equipped with a goniometer making it possible to perform angular-dependent in-plane as well as out-of-plane FMR measurements, providing information about in-plane anisotropy fields, and two-magnon scattering (TMS) contribution to the relaxation of the magnetization.

Besides cavity FMR measurements, the samples were investigated by broadband FMR measurements. In-plane broadband FMR measurements were performed using a transmission

geometry coplanar waveguide (CPW) where a lock-in amplifier detection technique was used. A pair of homemade Helmholtz coils generating a low-frequency, low-amplitude magnetic field (211.5 Hz and 0.25 mT magnetic field amplitude) was used to modulate the rf signal which was detected by the lock-in amplifier. As in cavity FMR, each measurement was performed varying the dc magnetic field while keeping the microwave frequency constant. FMR spectra were recorded in the frequency range from 5 to 20 GHz in steps of 1 GHz.

A setup enabling out-of-plane FMR measurements was also utilized. Recording the FMR signal by applying the field out of plane with respect to the sample surface provides a TMS-free FMR signal. For out-of-plane measurements a broadband vector network analyzer (VNA) was utilized. Two ports of the VNA were connected to a coplanar waveguide mounted in the air gap of an electromagnet.

III. RESULTS AND DISCUSSION

XRR measurements were performed to accurately determine thickness and roughness of the different layers in the Si/CFA(t_{CFA})/Ta samples. Figure 1 shows XRR spectra (symbols) together with simulated spectra (solid lines) for samples with different nominal CFA thickness. A three-layer model CFA/Ta/Ta₂O₅ was used in the simulations, since previous studies using x-ray photoelectron spectroscopy [17] and transmission electron microscopy [24] have shown that the top part of the Ta layer becomes oxidized, yielding Ta and Ta₂O₅ layers with thicknesses of about 2.5 and 2.2 nm, respectively. The results of the simulations are summarized in Table I. The results of the simulations show that the CFA thickness matches quite well with the nominal thickness and that differences in interface roughness between samples are small.

Figure 2 shows in-plane magnetization versus field curves for samples with different CFA thickness; for sake of clarity results are only shown for three samples. All samples exhibit rectangular hysteresis curves with small coercivity values; the coercivity was found to be weakly CFA thickness dependent

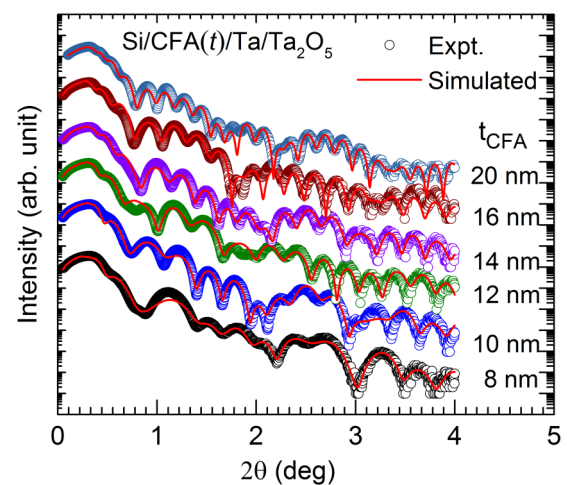


FIG. 1. X-ray reflectivity spectra recorded for Si/CFA(t_{CFA})/Ta/Ta₂O₅ thin films. Symbols correspond to experimental spectra and solid lines represent simulated curves.

TABLE I. Thickness and roughness values (σ) of the different layers in CFA/Ta/Ta₂O₅ films extracted from the simulation of the experimental XRR data.

t_{CFA} (nm)	σ (nm) ± 0.06	t_{CFA} (nm) ± 0.03	σ (nm) ± 0.06	t_{Ta} (nm) ± 0.03	σ (nm) ± 0.03	$t_{\text{Ta}_2\text{O}_5}$ (nm) ± 0.06	σ (nm) ± 0.03
8	0.21	8.54	0.34	2.37	0.20	2.26	0.28
10	0.35	10.88	0.60	2.62	0.19	2.42	0.34
12	0.38	12.20	0.55	2.59	0.37	2.16	0.50
14	0.28	14.32	0.46	2.42	0.47	2.15	0.41
16	0.20	16.03	0.55	2.50	0.45	2.19	0.31
20	0.22	20.22	0.43	2.45	0.31	2.25	0.13

and varied in the range 0.53–0.87 kA/m (0.65–1.10 mT). The inset shows the magnetization curve for one sample ($t_{\text{CFA}} = 20$ nm) applying the magnetic field out of plane with respect to the film surface; all samples exhibit similar out-of-plane magnetization curves. The saturation magnetization is best determined from the saturation field; the saturation magnetization determined in this way indicates a weakly CFA thickness-dependent value for the saturation magnetization ($\mu_0 M_s$) with values of about 1.10 T. These values are in good agreement with previously determined values for CFA films deposited by ion beam sputtering on Si substrates. The thickness-dependent saturation magnetization clearly demonstrates the absence of interfacial dead layers in these samples.

The in-plane angle-dependent cavity FMR data were analyzed using the following equation [25]:

$$f = \frac{\gamma \mu_0}{2\pi} \left([H_r \cos(\phi_H - \phi_M) + H_c \cos 4(\phi_M - \phi_C)] + H_u \cos 2(\phi_M - \phi_u) \right) \{ H_r \cos(\phi_H - \phi_M) + M_{\text{eff}} + \frac{H_c}{4} [3 + \cos 4(\phi_M - \phi_C)] + H_u \cos^2(\phi_M - \phi_u) \}^{1/2}, \quad (1)$$

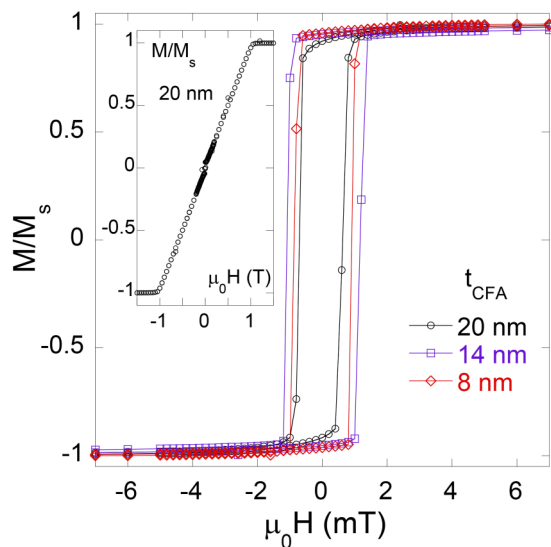


FIG. 2. In-plane magnetization normalized with the saturation magnetization versus field for CFA films with different thickness. The inset shows the normalized out-of-plane magnetization versus field for the CFA film with 20 nm thickness.

where H_r is the resonance field, f is the cavity microwave frequency, and $\gamma = \frac{g\mu_B}{\hbar}$ is the gyromagnetic ratio. Here, g is the Landé spectroscopic splitting factor, μ_B the Bohr magneton, and \hbar is the reduced Planck's constant. With respect to the [100] direction of the Si substrate, in-plane directions of the magnetic field, magnetization, uniaxial, and cubic anisotropies are given by ϕ_H , ϕ_M , ϕ_u and ϕ_C , respectively. $H_u = \frac{2K_u}{\mu_0 M_s}$ and $H_c = \frac{2K_c}{\mu_0 M_s}$ correspond to the uniaxial and cubic anisotropy fields, respectively, with K_u and K_c being the uniaxial and cubic magnetic anisotropy constants, respectively. $M_{\text{eff}} = M_s - H_k^\perp$ is the effective magnetization, where H_k^\perp is the perpendicular anisotropy field of the film. Here M_{eff} , H_c , and H_u are used as fitting parameters. Figure 3 shows H_r versus ϕ_H extracted from the angular-dependent FMR measurements together with fits according to Eq. (1), clearly revealing a dominant twofold uniaxial in-plane magnetic anisotropy. Using $g = 2.10$, a value which is in accord with values extracted from broadband FMR measurements, $\mu_0 M_{\text{eff}}$ shows small variation between samples taking values in the range 1.00–1.02 T. The results for the effective magnetization are close to the values extracted for the saturation magnetization (cf. inset in Fig. 2), showing that the perpendicular anisotropy field is negligibly small for the samples studied here. The uniaxial anisotropy field $\mu_0 H_u$ exhibits a decreasing trend with increasing CFA thickness, with values in the range 2.20–3.90 mT, while the cubic anisotropy field values are less than one-tenth of the uniaxial anisotropy field values.

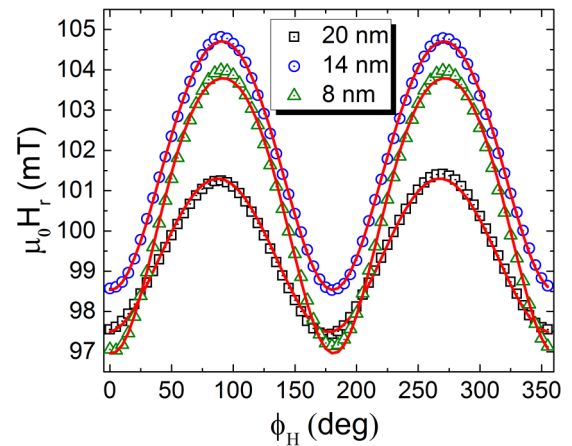


FIG. 3. Resonance field $\mu_0 H_r$ versus magnetic field rotation angle ϕ_H obtained from cavity FMR measurements. Symbols are experimental data points and lines are fits to Eq. (1).

The recorded FMR spectra linewidth have the following different contributions:

$$\mu_0 \Delta H = \mu_0 \Delta H^{inh} + \mu_0 \Delta H^{G+sp} + \mu_0 \Delta H^{mosaic} + \mu_0 \Delta H^{TMS}. \quad (2)$$

In the following we will discuss all four contributions in the linewidth. $\mu_0 \Delta H^{inh}$ is the frequency-independent sample inhomogeneity contribution, while $\mu_0 \Delta H^{G+sp} = 4\pi \alpha_{\text{eff}} f / \gamma \Phi$ is the Gilbert and spin-pumping damping contribution. Here, α_{eff} and Φ are the effective damping constant and a correction factor due to the field dragging effect. For the in-plane configuration $\Phi = \cos(\phi_M - \phi_H)$ and for the out-of-plane, $\Phi = \cos(\theta_M - \theta_H)$, where ϕ_H is the magnetic field azimuthal angle with respect to the in-plane crystallographic [100] direction, and θ_H is the polar angle of the magnetic field. $\phi_M(\theta_M)$ is the azimuthal (polar) angle of sample magnetization. This field dragging term enhances damping, but vanishes along the easy and hard axes (its presence in our studied samples is minute and will not be discussed further). The third term $\mu_0 \Delta H^{mosaic} = \frac{\partial H_r}{\partial \phi_H} \Delta \phi_H + \frac{\partial H_r}{\partial \theta_H} \Delta \theta_H$ is due to sample mosaicity [14,26]. This contribution to the linewidth originates from variation of crystallite orientations in the films, and from thickness variations. These microscopic variations result in spatial variations of the anisotropy fields and consequently

slight variations in the resonance field for different regions. This contribution is present in our studied samples. The last term $\mu_0 \Delta H^{TMS}$ is the two-magnon scattering (TMS) contribution. The TMS is a process where the $q = 0$ magnon scatters into a degenerate magnon with wave vector $\vec{q} \neq 0$. Arias and Mills have formulated a theoretical model where lattice geometrical defects induce magnetic inhomogeneity and yield two-magnon scattering [27]. Later Woltersdorf and Heinrich formulated a model including both isotropic and anisotropic angle-dependent TMS contributions to the linewidth [28]. For the in-plane configuration, which is discussed here, the TMS depends on the in-plane direction of the applied magnetic field relative to the principal in-plane crystallographic direction of the film. Angle-dependent TMS contributions appear when the scattering centers are anisotropic, e.g. self-assembled networks of misfit dislocations result in a fourfold angular dependence due to effective channeling of scattered spin waves. Moreover, rectangular surface defects cause a $(\cos 2\phi_H)^2$ angular dependence. A slightly different symmetry of surface defects results in a \vec{q} wave-vector-dependent $(\cos 2\varphi)^4$ angular dependence, where $\varphi = \phi_M + \psi$; ψ is the angle between the magnetization vector and \vec{q} . Therefore, combining the Arias and Mills, and Woltersdorf and Heinrich models of TMS, the angular dependence of TMS can be expressed as

$$\mu_0 \Delta H^{TMS} \propto \frac{\Gamma}{\Phi} \sin^{-1} \sqrt{\left(\sqrt{\omega^2 + \left(\frac{\omega_0}{2}\right)^2} - \frac{\omega_0}{2} \right) / \left(\sqrt{\omega^2 + \left(\frac{\omega_0}{2}\right)^2} + \frac{\omega_0}{2} \right)} \int w(\psi) (\cos 2\phi_H)^2 (\cos 2\varphi)^4 d\psi, \quad (3)$$

where Γ is the intensity of the TMS, $w(\psi)$ is a weighting parameter along the path of the TMS scattering lobes $\vec{q}(\psi)$, $\omega_0 = \gamma \mu_0 M_{\text{eff}}$, and ω is angular frequency.

The angle-dependent linewidth obtained from cavity FMR measurements was fitted using Eqs. (2) and (3) to extract the thickness-dependent TMS linewidth contribution, shown in Fig. 4. Since broadband in-plane FMR results do not indicate any field dragging effect, implying $\phi_M = \phi_H$, both ΔH^{inh} and ΔH^{G+sp} correspond to isotropic contributions to the linewidth and the exact value of both cannot be extracted from this analysis. However, the weighting-factor-dependent TMS intensity Γ can be extracted from the fitting. Γ increases from 2.6 to 4.5 mT, decreasing the CFA thickness from 20 to 8 nm, clearly indicating the presence of a thickness-dependent TMS linewidth contribution in our studied samples.

In-plane broadband FMR measurements were performed with the magnetic field applied along the easy axis of the films. Recorded FMR spectra were fitted to the expression [29]

$$\frac{dA}{dH} \propto \frac{2(H - H_r) \frac{\Delta H}{2}}{\left[\left(\frac{\Delta H}{2}\right)^2 + (H - H_r)^2 \right]^2} - \frac{\left[\left(\frac{\Delta H}{2}\right)^2 - (H - H_r)^2 \right]}{\left[\left(\frac{\Delta H}{2}\right)^2 + (H - H_r)^2 \right]^2}, \quad (4)$$

where $\frac{dA}{dH}$ is the magnetic field derivative of the microwave absorption signal. The full width at half maximum linewidth ΔH and resonance field H_r were used as fitting parameters. Figure 5 shows FMR spectra at different frequencies for

the $t_{\text{CFA}} = 16$ nm sample and Fig. 6(a) shows ΔH versus frequency for CFA samples with different thickness (leaving out results for two samples for the sake of clarity). The inset in Fig. 5 shows H_r versus frequency for the $t_{\text{CFA}} = 16$ nm sample together with a fit of the experimental data to Eq. (1); the results for other samples are very similar and plotting more

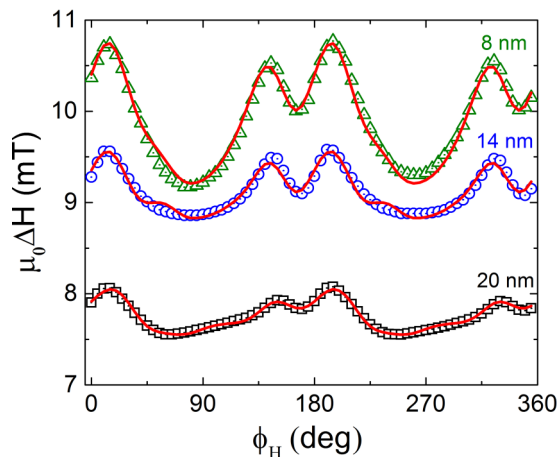


FIG. 4. Linewidth $\mu_0 \Delta H$ versus magnetic field rotation angle ϕ_H obtained from cavity FMR measurements. Symbols are experimental data points and lines are fits to Eqs. (2) and (3). The extracted TMS contributions to the linewidth are 2.6, 3.8, and 4.5 mT for the 20-, 14-, and 8-nm-thick CFA samples, respectively.

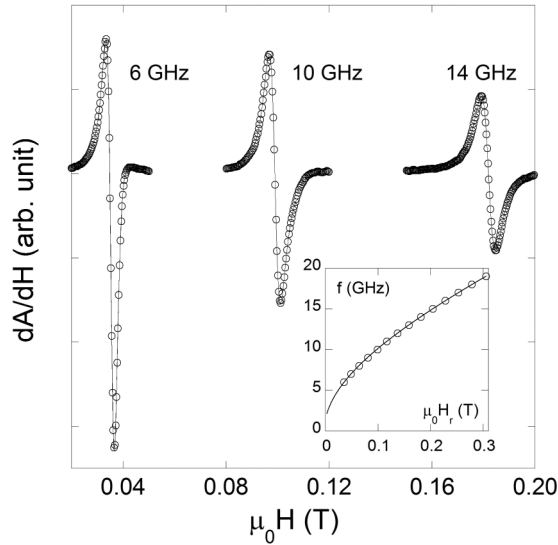


FIG. 5. In-plane FMR spectra for the 16-nm-thick CFA film. Symbols are experimental data and solid lines are fits to Eq. (4). The inset shows frequency versus resonance field for the same sample. Symbols are experimental data and the solid line is a fit to Eq. (1).

than one curve in the graph it is very difficult to distinguish one curve from the other by eye. Using g as a free parameter, one obtains $g = 2.10$, while $\mu_0 M_{\text{eff}}$ takes values in the range 1.00–1.05 T. The ΔH versus frequency data were fitted to the expression [29]

$$\mu_0 \Delta H = \frac{4\pi\alpha_{\text{eff}}}{\gamma} f + \mu_0 \Delta H_0, \quad (5)$$

where α_{eff} is the effective damping parameter, which for the in-plane configuration, in addition to the intrinsic Gilbert damping, contains both a TMS contribution and a contribution due to spin pumping into the Ta layer, and ΔH_0 ($=\Delta H^{\text{inh}} + \Delta H^{\text{mosaic}}$) is a sum of the frequency-independent inhomogeneity and mosaicity contributions to the linewidth. Extracted α_{eff} values versus CFA thickness are shown in Fig. 6(b). The extracted values of α_{eff} increase with decreasing CFA layer thickness, indicating a $\frac{1}{t_{\text{CFA}}}$ dependence. The extracted $\mu_0 \Delta H_0$ values vary in the range 1.2–2.5 mT, being smaller for $t_{\text{CFA}} < 12$ nm (1.2–1.6 mT).

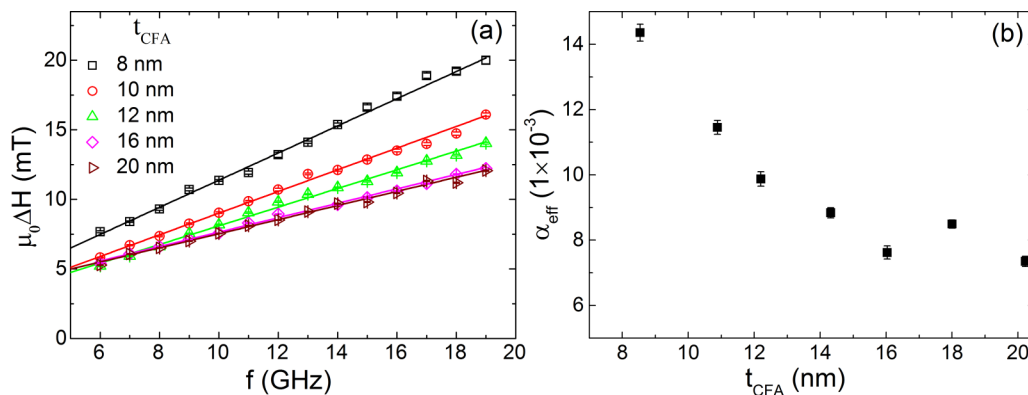


FIG. 6. (a) $\mu_0 \Delta H$ versus f (a) from in-plane FMR measurements for samples with different CFA thickness. Symbols correspond to experimental data and lines are fits to Eq. (5). (b) α_{eff} versus t_{CFA} .

Broadband out-of-plane FMR measurements were performed in the frequency range from 5 to 17 GHz. During these measurements the VNA was utilized to record the frequency and magnetic field dependence of the complex transmission parameter S_{21} of the microwave signal. Typical results for the real and imaginary parts of S_{21} for the $t_{\text{CFA}} = 20$ nm sample are given in Fig. 7. Recorded S_{21} spectra were fitted to the following set of equations [30]:

$$S_{21}(H, t) = S_{21}^0 + Dt + \frac{\chi(H)}{\tilde{\chi}_0},$$

$$\chi(H) = \frac{M_{\text{eff}}(H - M_{\text{eff}})}{(H - M_{\text{eff}})^2 - H_{\text{eff}}^2 - i\Delta H(H - M_{\text{eff}})}. \quad (6)$$

In these equations S_{21}^0 is the nonmagnetic contribution to S_{21} , $\chi(H)$ is the complex susceptibility of the magnetic film, and $\tilde{\chi}_0$ is an imaginary function of the frequency and film thickness. The term Dt accounts for a linear drift of the recorded S_{21} signal and $H_{\text{eff}} = 2\pi f/\gamma\mu_0$.

M_{eff} and the Landé g factor can be extracted by fitting the H_r versus frequency results to the expression

$$\mu_0 H_r = \frac{2\pi f}{\gamma} + \mu_0 M_{\text{eff}}. \quad (7)$$

Typical results are shown in Fig. 8(a) for the $t_{\text{CFA}} = 8$ - and 20-nm samples. Following the method outlined in Ref. [30], $\mu_0 M_{\text{eff}}$ and g increase slightly and take values in the range 1.15–1.20 T and 2.07–2.13, respectively. Figure 8(b) shows ΔH versus f extracted from out-of-plane FMR results, again indicating an increase of α_{eff} with decreasing thickness of the CFA layer. The damping parameter extracted in this way includes the intrinsic Gilbert contribution (α_G) and the contribution due to spin pumping (α_{sp}); $\alpha_{\text{eff}} = \alpha_G + \alpha_{sp}$. Here we have ignored the radiative and eddy current contributions to the damping, which are expected to give a contribution $\lesssim 3 \times 10^{-4}$. The theoretical framework describing the relaxation of injected spins in the nonmagnetic layers, including the backflow of spin angular momentum from the nonmagnetic layers into the magnetic layer, was presented in Refs. [19,20]. The theory as derived is restricted to metals with a ratio of the spin-conserved to spin-flip scattering times (the spin-flip probability) $\epsilon = \tau_{el}/\tau_{SF} = (\lambda_{el}/\lambda_{SD})^2/3 \gtrsim 10^{-3}$, where λ_{el} and λ_{SD} are the mean free path and spin-diffusion length,

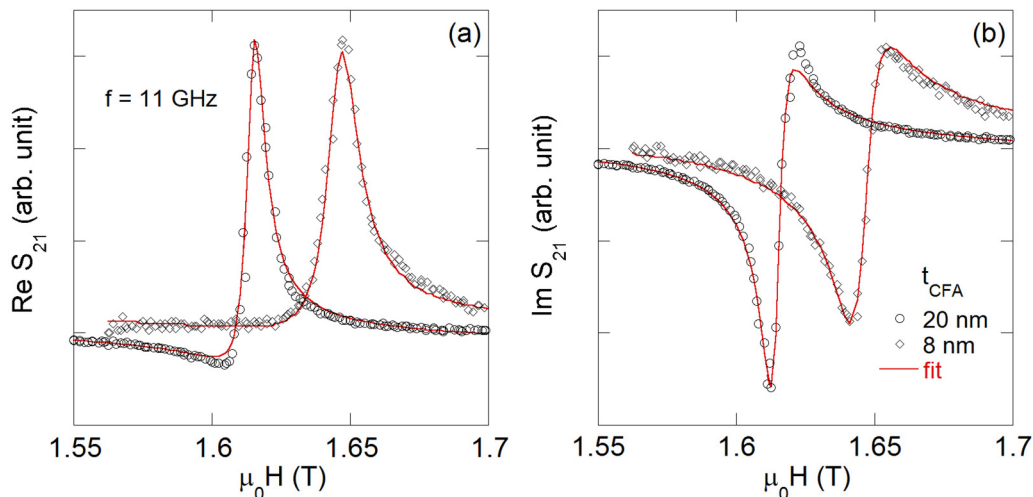


FIG. 7. Out-of-plane FMR spectra for 8- and 20-nm-thick CFA films showing (a) real and (b) imaginary parts of S_{21} . Symbols are experimental data and lines are fits to Eq. (6).

respectively. For a nonmagnetic metal to be an efficient spin sink, the requirement is $\epsilon \gtrsim 10^{-2}$ [20]. Using values for λ_{el} and λ_{SD} derived for ferromagnetic/ β -Ta bilayers ($\lambda_{el} = 0.5$ nm and $\lambda_{SD} = 2.5$ nm) [31], the value for the spin-flip probability becomes $\epsilon = 1.3 \times 10^{-2}$ indicating that the model is applicable to ferromagnetic/ β -Ta bilayers and that β -Ta acts as an efficient spin sink. In the simplest case, with only one interface, the extra contribution to the damping can be expressed as

$$\alpha_{sp} = \frac{g\mu_B g_{\text{eff}}^{\uparrow\downarrow}}{4\pi M_s t_{\text{CFA}}} \frac{1}{t_{\text{CFA}}}, \quad (8)$$

where $g_{\text{eff}}^{\uparrow\downarrow}$ is the real part of interfacial mixing conductance $g^{\uparrow\downarrow}$ in series with the normal-metal resistance. For the samples discussed here there are two interfaces, one between the CFA and Ta layers and one between the Ta and Ta_2O_5 layers. This implies that $g_{\text{eff}}^{\uparrow\downarrow}$ will be a function of the conductance at both interfaces, since spin relaxation is expected both in the Ta and Ta_2O_5 layers. Figure 9(a) shows α_{eff} extracted from out-of-plane FMR measurements versus $\frac{1}{t_{\text{CFA}}}$ together with a fit of the experimental data to Eq. (8). Using

$M_s = 915$ kA/m ($\mu_0 M_s = 1.15$ T) and $g = 2.10$, one obtains $g_{\text{eff}}^{\uparrow\downarrow} = (2.90 \pm 0.1) \times 10^{19}$ m $^{-2}$, which is comparable to the value obtained for a Pd/CoFe/Pd multilayer structure [32]. Using this value for the effective mixing conductance, it is now possible to disentangle the two contributions to α_{eff} ; Fig. 9(b) shows α_{eff} together with α_{sp} and α_G versus CFA layer thickness. The extracted value for the intrinsic Gilbert is $\alpha_G = 1.1 \pm 0.2 \times 10^{-3}$, which is in good agreement with previously determined values [17]. Moreover, assuming that the spin current is reflected at the β -Ta/ Ta_2O_5 interface and using the relation between the intrinsic and effective spin-mixing conductance $g_{\text{eff}}^{\uparrow\downarrow} = g^{\uparrow\downarrow}(1 - e^{-2t_{\text{Ta}}/\lambda_{SD}})$, where t_{Ta} is the thickness of the β -Ta layer and the exponential term within the brackets accounts for the backflow of spin angular momentum, one obtains $g^{\uparrow\downarrow} \approx 3.35 \times 10^{19}$ m $^{-2}$ for the intrinsic spin-mixing conductance.

The low Gilbert damping ($\leq 1 \times 10^{-3}$) and high spin-mixing conductance ($\geq 1 \times 10^{19}$ m $^{-2}$) observed for the CFA/ β -Ta bilayer system are key requirements for spin transfer torque magnetization switching and spin logic devices. However, efficient switching of magnetic memory and spin logic devices also requires a large interface transparency (T). The

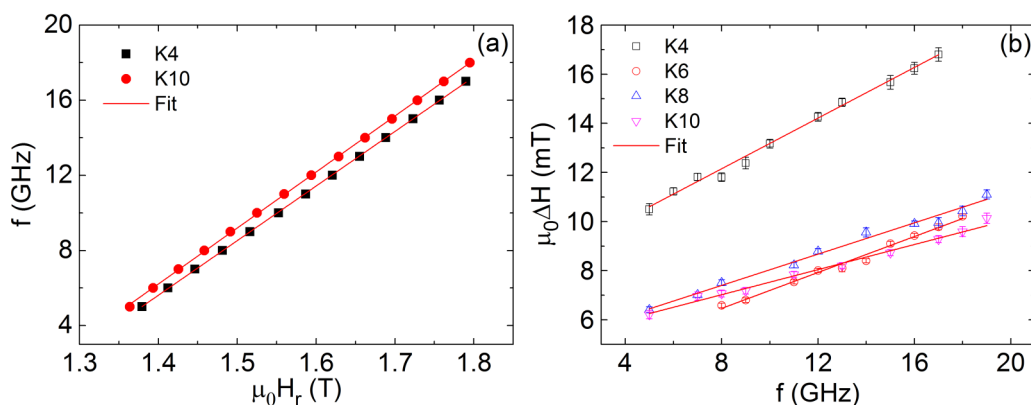


FIG. 8. f versus H_r (a) and $\mu_0 \Delta H$ versus f (b) from out-of-plane FMR measurements for samples with different CFA thickness. Symbols correspond to experimental data and lines are fits to Eqs. (7) and (5). Since error in H_r is negligible, no error bars are shown in (a).

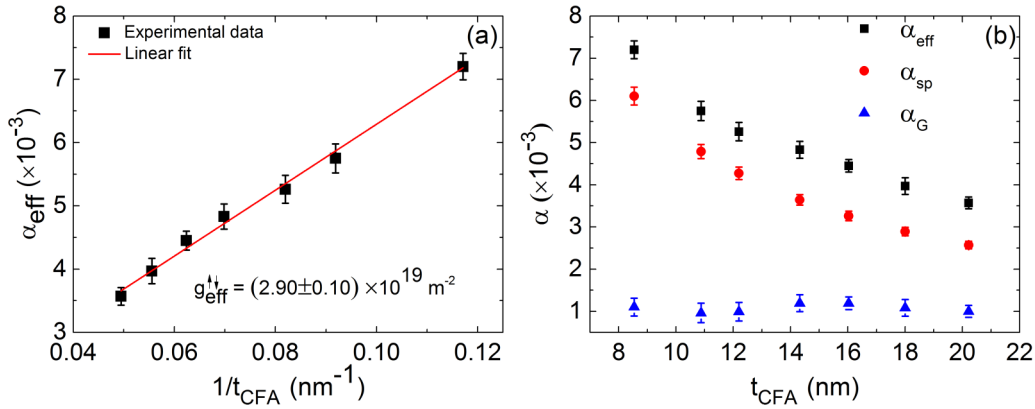


FIG. 9. (a) α_{eff} versus $\frac{1}{t_{\text{CFA}}}$ using data extracted from out-of-plane FMR measurements. Squares correspond to the experimental data and solid line fit to Eq. (8). (b) α_{eff} , spin-pumping contribution α_{sp} to damping and intrinsic Gilbert damping α_G versus t_{CFA} .

interface transparency in the CFA/ β -Ta bilayer system controls the flow of spin angular momentum across the interface and depends on the microscopic intrinsic and extrinsic interfacial factors, such as band structure mismatch, Fermi velocity, and interface imperfections, and can be expressed as [33]

$$T = \frac{g_{\text{eff}}^{\uparrow\downarrow} \tanh\left(\frac{t_{\text{CFA}}}{2\lambda_{\text{SD}}}\right)}{g_{\text{eff}}^{\uparrow\downarrow} \coth\left(\frac{t_{\text{Ta}}}{\lambda_{\text{SD}}}\right) + \frac{\sigma_{\text{Ta}}\hbar}{\lambda_{\text{SD}}2e^2}}, \quad (9)$$

where $\sigma_{\text{Ta}} (= 5 \times 10^5 \Omega^{-1} \text{m}^{-1})$ is the conductivity of the β -Ta layer. The estimated value of the transparency for the CFA/ β -Ta interface is $\sim 68\%$. This T value is even higher than for FM/Pt interfaces [33], clearly indicating the significance of using the CFA/ β -Ta structure in innovative spin transfer torque devices.

IV. CONCLUSIONS

The effects of Co_2FeAl thickness covering the range 8–20 nm on the static and dynamic properties of Si/ $\text{Co}_2\text{FeAl}/\beta$ -Ta multilayers have been investigated. It was found that static properties like the saturation magnetization and coercivity were weakly thickness dependent, with values covering the range 900–950 kA/m and 0.53–0.87 kA/m, respectively. The in-plane uniaxial anisotropy field was determined from angle-dependent cavity FMR measurements, indicating a decreasing trend with increasing CFA thickness, with values covering the range 2.20–3.90 mT. Both in-plane and out-of-plane broadband

FMR measurements show that the effective damping parameter increases with decreasing thickness, indicating an enhancement of damping due to spin pumping into the nonmagnetic cap layer. The in-plane damping parameter is also affected by spin relaxation due to two-magnon scattering, resulting in a larger effective damping parameter as compared to the out-of-plane damping parameter. The out-of-plane effective damping parameter, being free from spin relaxation due to two-magnon scattering, was further analyzed to extract information about the effective spin-mixing conductance of the multilayer as well as to disentangle the contributions to the effective damping parameter, yielding $g_{\text{eff}}^{\uparrow\downarrow} = (2.90 \pm 0.10) \times 10^{19}$ and $\alpha_G = (1.1 \pm 0.2) \times 10^{-3}$. The high value of $g_{\text{eff}}^{\uparrow\downarrow}$ for the CFA/ β -Ta structure, at par with that of FM/Pt bilayers, in conjunction with $\sim 68\%$ interface transparency and low Gilbert damping ($\leq 1.1 \times 10^{-3}$) of CFA clearly makes the CFA/ β -Ta structure a promising building block for spin transfer torque devices.

ACKNOWLEDGMENTS

This work is supported by the Knut and Alice Wallenberg (KAW) Foundation, Grant No. KAW 2012.0031. S.H. acknowledges the Department of Science and Technology India for providing the the INSPIRE Fellowship (Grant No. IF140093) grant.

S.A. and A.K. contributed equally to this work.

- [1] J. C. Slonczewski, Current-driven excitation of magnetic multilayers, *J. Magn. Magn. Mater.* **159**, L1 (1996).
- [2] L. Berger, Emission of spin waves by a magnetic multilayer traversed by a current, *Phys. Rev. B* **54**, 9353 (1996).
- [3] I. Galanakis, P. H. Dederichs, and N. Papanikolaou, Slater-Pauling behavior and origin of the half-metallicity of the full-Heusler alloys, *Phys. Rev. B* **66**, 174429 (2002).
- [4] S. Picozzi, A. Continenza, and A. J. Freeman, Co_2MnX ($X = \text{Si, Ge, Sn}$) Heusler compounds: An *ab initio* study of their structural, electronic, and magnetic properties at zero and elevated pressure, *Phys. Rev. B* **66**, 094421 (2002).
- [5] S. Trudel, O. Gaier, J. Hamrle, and B. Hillebrands, Magnetic anisotropy, exchange and damping in cobalt-based full-Heusler compounds: An experimental review, *J. Phys. D: Appl. Phys.* **43**, 193001 (2010).
- [6] W. Wang, E. Liu, M. Kodzuka, H. Sukegawa, M. Wojcik, E. Jedryka, G. H. Wu, K. Inomata, S. Mitani, and K. Hono, Coherent tunneling and giant tunneling magnetoresistance in $\text{Co}_2\text{FeAl}/\text{MgO}/\text{CoFe}$ magnetic tunneling junctions, *Phys. Rev. B* **81**, 140402(R) (2010).
- [7] W. Wang, H. Sukegawa, and K. Inomata, Temperature dependence of tunneling magnetoresistance in epitaxial magnetic tunnel junctions using a Co_2FeAl Heusler alloy electrode, *Phys. Rev. B* **82**, 092402 (2010).
- [8] M. Belmeguenai, H. Tuzcuoglu, M. S. Gabor, T. Petrisor, C. Tiusan, F. Zighem, S. M. Chérif, and P. Moch, Co_2FeAl Heusler

- thin films grown on Si and MgO substrates: Annealing temperature effect, *J. Appl. Phys.* **115**, 043918 (2014).
- [9] B. Sun, K. Kim, N. Leibing, and S. Serrano-Guisan, Structural and magnetic properties of epitaxial Co₂FeAl films grown on MgO substrates for different growth temperatures, *Acta Mater.* **60**, 6714 (2012).
- [10] S. Mizukami, D. Watanabe, M. Oogane, Y. Ando, Y. Miura, M. Shirai, and T. Miyazaki, Low damping constant for Co₂FeAl Heusler alloy films and its correlation with density of states, *J. Appl. Phys.* **105**, 07D306 (2009).
- [11] G. Ortiz, M. S. Gabor, T. Petrisor, Jr., F. Boust, F. Issac, C. Tiusan, M. Hehn, J. F. Bobo, and T. Petrisor, Static and dynamic magnetic properties of epitaxial Co₂FeAl Heusler alloy thin films, *J. Appl. Phys.* **109**, 07D324 (2011).
- [12] H. Sukegawa, Z. Wen, K. Kondou, S. Kasai, S. Mitani, and K. Inomata, Spin-transfer switching in full-Heusler Co₂FeAl-based magnetic tunnel junctions, *Appl. Phys. Lett.* **100**, 182403 (2012).
- [13] W. Wang, E. Liu, Y. Du, J. Chen, G. Wu, H. Sukegawa, S. Mitani, and K. Inomata, Thickness-dependent structural, magnetic and transport properties of epitaxial Co₂FeAl Heusler alloy thin films, [arXiv:1210.5807](https://arxiv.org/abs/1210.5807).
- [14] M. Belmeguenai, H. Tuzcuoglu, M. S. Gabor, T. Petrisor, C. Tiusan, D. Berling, F. Zighem, T. Chauveau, S. M. Chérif, and P. Moch, Co₂FeAl thin films grown on MgO substrates: Correlation between static, dynamic, and structural properties, *Phys. Rev. B* **87**, 184431 (2013).
- [15] X. G. Xu, D. L. Zhang, X. Q. Li, J. Bao, Y. Jiang, and M. B. A. Jalil, Synthetic antiferromagnet with Heusler alloy Co₂FeAl ferromagnetic layers, *J. Appl. Phys.* **106**, 123902 (2009).
- [16] M. Belmeguenai, H. Tuzcuoglu, M. Gabor, T. Petrisor, C. Tiusan, D. Berling, F. Zighem, and S. Mourad Chérif, Magnetic and structural properties of Co₂FeAl thin films grown on Si substrate, *J. Magn. Magn. Mater.* **373**, 140 (2015).
- [17] S. Husain, S. Akansel, A. Kumar, P. Svedlindh, and S. Chaudhary, Growth of Co₂FeAl Heusler alloy thin films on Si(100) having very small Gilbert damping by ion beam sputtering, *Sci. Rep.* **6**, 28692 (2016).
- [18] X. Liu, W. Zhang, M. J. Carter, and G. Xiao, Ferromagnetic resonance and damping properties of CoFeB thin films as free layers in MgO-based magnetic tunnel junctions, *J. Appl. Phys.* **110**, 033910 (2011).
- [19] Y. Tserkovnyak, A. Brataas, and G. E. W. Bauer, Enhanced Gilbert Damping in Thin Ferromagnetic Films, *Phys. Rev. Lett.* **88**, 117601 (2002).
- [20] Y. Tserkovnyak, A. Brataas, and G. E. W. Bauer, Spin pumping and magnetization dynamics in metallic multilayers, *Phys. Rev. B* **66**, 224403 (2002).
- [21] M. J. Hurben and C. E. Patton, Theory of two magnon scattering microwave relaxation and ferromagnetic resonance linewidth in magnetic thin films, *J. Appl. Phys.* **83**, 4344 (1998).
- [22] R. Arias and D. L. Mills, Extrinsic contributions to the ferromagnetic resonance response of ultrathin films, *Phys. Rev. B* **60**, 7395 (1999).
- [23] N. Behera, A. Kumar, S. Chaudhary, and D. K. Pandya, Two magnon scattering and anti-damping behavior in a two-dimensional epitaxial TiN/Py(t_{Py})/β-Ta(t_{Ta}) system, *RSC Adv.* **7**, 8106 (2017).
- [24] N. Behera, P. Guha, D. K. Pandya, and S. Chaudhary, Capping layer (CL) induced antidamping in CL/Py/β-W system (CL: Al, β-Ta, β-W), *ACS Appl. Mater. Interfaces* **9**, 31005 (2017).
- [25] H. Pandey, P. C. Joshi, R. P. Pant, R. Auluck, and R. C. Budhani, Evolution of ferromagnetic and spin-wave resonance with crystalline order in thin films of full-Heusler alloy Co₂MnSi, *J. Appl. Phys.* **111**, 023912 (2012).
- [26] K. Zakeri, J. Lindner, I. Barsukov, R. Meckenstock, M. Farle, U. von Hörsten, H. Wende, W. Keune, J. Rocker, S. S. Kalarickal, K. Lenz, W. Kuch, K. Baberschke, and Z. Frait, Spin dynamics in ferromagnets: Gilbert damping and two-magnon scattering, *Phys. Rev. B* **76**, 104416 (2007).
- [27] R. Arias and D. L. Mills, Extrinsic contributions to the ferromagnetic resonance response of ultrathin films, *J. Appl. Phys.* **87**, 5455 (2000).
- [28] G. Woltersdorf and B. Heinrich, Two-magnon scattering in a self-assembled nanoscale network of misfit dislocations, *Phys. Rev. B* **69**, 184417 (2004).
- [29] G. Woltersdorf, Spin-pumping and two-magnon scattering in magnetic multilayers, Ph.D. thesis, Simon Fraser University, 2004.
- [30] H. T. Nembach, T. J. Silva, J. M. Shaw, M. L. Schneider, M. J. Carey, S. Maat, and J. R. Childress, Perpendicular ferromagnetic resonance measurements of damping and Landé f-factor in sputtered (Co₂Mn)_{1-x}Ge thin films, *Phys. Rev. B* **84**, 054424 (2011).
- [31] G. Allen, S. Manipatruni, D. E. Nikonov, M. Doczy, and I. A. Young, Experimental demonstration of the coexistence of spin Hall and Rashba effects in β-tantalum/ferromagnetic bilayers, *Phys. Rev. B* **91**, 144412 (2015).
- [32] J. M. Shaw, H. T. Nembach, and T. J. Silva, Determination of spin pumping as a source of linewidth in sputtered Co₉₀Fe₁₀/Pd multilayers by use of broadband ferromagnetic resonance spectroscopy, *Phys. Rev. B* **85**, 054412 (2012).
- [33] C.-F. Pai, Y. Ou, L. H. Vilela-Leao, D. C. Ralph, and R. A. Buhrman, Dependence of the efficiency of spin Hall torque on the transparency of Pt/ferromagnetic layer interfaces, *Phys. Rev. B* **92**, 064426 (2015).